J Mater Sci (2018) 53:7648–7656

Energy materials

Influence of chemical functionalization on the thermoelectric properties of monodispersed single-walled carbon nanotubes

Mingxing Piao[1,*], Chaolong Li[1], Jin Chu[1], Xiao Wang[1], Heng Zhang[1], and Yao Chi[1]

[1] *Key Laboratory of Multi-Scale Manufacturing Technology, Chongqing Institute of Green and Intelligent Technology, Chinese Academy of Sciences, Chongqing 400714, People's Republic of China*

Received: 1 December 2017
Accepted: 22 January 2018
Published online: 30 January 2018

ABSTRACT

Single-walled carbon nanotubes (SWCNTs) networks have attracted great attention for electronic and energy-harvesting applications, including thermoelectric (TE) devices. However, the simultaneous production of metallic SWCNTs (m-SWCTNs) and semiconducting SWCNTs (s-SWCNTs) randomly with distinct electronic structures always hinders the specific usage. The investigation of the influence of different electronic structures by nature or artificially on the TE performances of monodispersed SWCNTs is significative. In this report, high purity of separated m- and s-SWCNTs was chemically functionalized with 4-bromobenzene diazonium tetrafluoroborate, leading to the hybridization of *C* atoms changed from sp^2 to sp^3. The influence of the electronic type of SWCNTs on the TE properties as a function of the modifier agent was systematically investigated. As a consequence, the maximum power factor of s-SWCNTs networks was as high as 244.2 μW m^{-1} K^{-2} under the optimal condition, whereas it was only 5.3 μW m^{-1} K^{-2} for m-SWCNTs networks. In addition, grafting of functional groups onto the sidewall of nanotubes was predicted to further decrease the thermal conductivity, which is beneficial to increment of the *ZT* values. Based on these results, we believe that the pure s-SWCNTs and a variety of chemically functionalized composites have great potential as candidate for TE applications.

Introduction

Thin films of entangled single-walled carbon nanotubes (SWCNTs) are widely investigated for applications in variety of technologies such as photovoltaics [1], organic light-emitting diodes [2], flat-panel displays [3], printed electronics [4, 5], biosensors [6] and thermoelectric (TE) power generators [7, 8]. The ease of solution processing SWCNTs as thin films and their mechanical flexibility and compatibility with other electronic active organic

Address correspondence to E-mail: piaomx@cigit.ac.cn

https://doi.org/10.1007/s10853-018-2063-4

materials motivate research to further improve their electronic and TE properties. Many factors can influence the charge and heat transports of SWCNTs networks, including network morphology [9], chemical doping [10, 11] surface defects [12] and so on. Individual nanotube is either metallic SWCNTs (m-SWCNTs) or semiconducting SWCNTs (s-SWCNTs) which depends on its chirality [13]. Since the m- and s-SWCNTs possess diverse band structures, the electrical conductivity and Seebeck coefficient which closely related with the density of state (*DOS*) [14, 15] are predicted to be discrepant. Therefore, the TE properties of SWCNTs networks can be significantly influenced by the electronic types of nanotubes. Furthermore, in order to fully use the potential of SWCNTs networks in TE devices, it is crucial to utilize monodispersed nanotubes that improve the electronic homogeneity to achieve optimal performance. Recent years, achieved progress in the efficient separation of SWCNTs by electronic type [16–19] allows investigations on the TE properties of as-deposited m- and s-SWCNTs networks.

According to previously reported literatures, physical treatment [20, 21] or chemical functionalization [22–24] of nanotubes played an important role on the TE properties of SWCNTs networks. Unfortunately, most attentions were paid to a heterogeneous mixture of m-SWCNTs and s-SWCNTs in an approximate ratio of 1:2 and the influence of electronic type of SWCNTs on the TE properties was rarely reported. Actually, due to the distinct different energy band structure, it was expected the monodispersed SWCNTs networks appear quite different TE properties [25, 26]. On the other hand, there always exist different kinds of defects on the nanotubes naturally or artificially, which affect the original properties or produce novel properties of nanotubes [27, 28]. Chemical functionalization is one of the most frequent ways to alter the intrinsic properties of nanotubes deliberately. Hence, it is worth and interesting to investigate the influence of chemical functionalization on the TE properties of m- and s-SWCNTs networks.

In this report, the monodispersed SWCNTs networks were prepared with pure m- and s-SWCNTs dispersions by using facile vacuum filtration technique, and their TE properties were studied, respectively. 4-Bromobenzene diazonium tetrafluoroborate (4-BBDT), which demonstrated chemical reaction selectivity on the electronic type of SWCNTs [29], was chosen as a typical modifier agent to chemical functionalization of the m- and s-SWCNTs. Then, the influence of electronic type of SWCNTs on the TE properties as a function of 4-BBDT content was systematically investigated. It was found the maximum power factor of s-SWCNTs networks was as high as 244.2 $\mu W\ m^{-1}\ K^{-2}$ under the optimized condition, which was better than most of organic TE materials. On the contrast, the value was only 5.3 $\mu W\ m^{-1}\ K^{-2}$ for m-SWCNTs networks. Following these results, we believe that the pure s-SWCNTs and a variety of relevant chemically functionalized composites have great potential as candidate for future TE applications.

Materials and methods

The monodispersed m- and s-SWCNTs dispersions were purchased from NanoIntegris Inc. that are synthesized by Arc discharge method and separated by a density gradient ultracentrifugation technique with the purity more than 99%. The separated m- and s-SWCNTs were dispersed well in water through utilizing 1% (w/v) of proprietary ionic surfactant in NanoIntegris Inc. with a concentration of 0.01 mg ml^{-1}. According to the database supplied by NanoIntegris Inc. obtained from the statistical results of atomic force microscopy (AFM), the mean length of the s-SWCNTs was 1 μm, which was 2 times longer than that of m-SWCNTs and the mean diameter of both types was 1.4 nm. 4-BBDT and sodium hydroxide (NaOH) were purchased from Aldrich and applied directly without further purification. Deionized water obtained from ultrapure water machine (ATSelem 1810A) was used in all of the experiments.

To chemical functionalization on the sidewall of s-SWCNTs, 100 mg 4-BBDT powder was firstly dissolved in water to obtain a homogeneous solution (0.1 mg ml^{-1}) by adjusting pH = 10 with NaOH. Then, different volumes of 4-BBDT solution (3.6, 8.3 and 16.5 ml) were added into 6 ml of s-SWCNTs suspensions following vigorous magnetic stirring for 30 min at room temperature. After that, thin films were prepared through vacuum filtrating the mixture solutions using a polycarbonate (PC) membrane (pore size 0.4 μm, from Millipore). The surfactant was removed by rinsing with deionized water several times. Finally, thin films of s-SWCNTs networks functionalized with 4-BBDT were dried in an oven at

80 °C for 1 h to evaporate the water completely. The molar ratios between 4-BBDT and SWCNTs were adjusted to be 0.3, 0.7 and 1.4, respectively (signed with $N_{4\text{-BBDT}}/\ N_{s\text{-SWCNT}} = 0.3,\ 0.7,\ 1.4$). The same procedure was carried out on m-SWCNTs suspension to investigate the influence of the electronic type on the TE properties after chemical functionalized induced by 4-BBDT. Furthermore, the pristine m- and s-SWCNTs networks without chemical functionalization were also prepared by employing the typical vacuum filtration technique.

The surface morphology of SWCNTs networks was analyzed using scanning electron microscope (SEM, Hitachi S-4800). An Ar^+ ion laser (514 nm) was used as a source in the Jobin–Yvon HR800UV Raman spectrometer to probe the functionalization degree of the SWCNTs networks. The absorption spectrum was obtained with spectrometer (Cary 5000). AFM (Park system, XE-100) analysis was performed to observe the morphology of SWCNTs networks. The electrical conductivity was obtained with four-probe method. The SWCNTs thin films were cut into strips, typically 20 × 20 mm. Each sample was pressure-contacted with four parallel metallic Pt wires to perform the standard four-probe measurement at room temperature. Current–voltage (I–V) sweeps were operated using a Keithley 238 as the current source and a 34401A multimeter from Hewlett-Packard for the voltage measurement. Electrical conductance was obtained by taking the slope of the I–V curve and converting it into electrical conductivity by multiplying the geometric factor. To reduce the measurement error caused by fluctuations from sample to sample, ten different sample stripes were tested. To determine the Seebeck coefficient, a temperature gradient (ΔT) was created along the film strip by heating one end of the strip and leaving the other end exposed to air. Two platinum (Pt 100 Ω) resistors were clamped with electrical contacts at the ends of the strips to measure the sample temperature. The Seebeck coefficient was calculated from the potential difference (ΔV) generated by ΔT using $S = -\Delta V/\Delta T$.

Results and discussion

Firstly, the monodispersed m- and s-SWCNTs networks deposited on the PC membrane were characterized. The digital photographs of each type of SWCNTs networks are displayed in inset of Fig. 1a, b. From macroscopic view, each type of SWCNTs networks can be distinguished easily by color. The m-SWCNTs networks visually appeared to be green color, and s-SWCNTs networks showed brown color. The microscopic structure of the networks was observed from the SEM images, as displayed in Fig. 1a, b. The surface morphology appeared similar for both types of SWCNTs networks. The long SWCNTs bundles were formed with diameters around 5–20 nm. They were interwoven with each other and formed uniform impurity free networks. The absorption spectrum was performed to determine the purity of each type of SWCNTs, as shown in Fig. 1c. In the case of s-SWCNTs, two absorption peaks were clearly separated with a deep plateau, corresponding to the electronic transitions of the second-order semiconducting transitions (S_{22}, 900–1270 nm) and third-order semiconducting transitions (S_{33}, 450–630 nm) [30, 31]. On the contrary, one main absorption peak, reflected the first-order metallic transitions (M_{11}, 600–850 nm), was observed without any side bands in the spectrum of m-SWCTNs, indicating a high purity of metallic and semiconducting species. As-prepared monodispersed SWCNTs networks were also characterized by Raman spectroscopy. Figure 1d exhibits the typical Raman spectra of SWCNTs with the laser energy at 1.96 eV. Both types of SWCNTs showed radial breathing (RBM) mode, D mode, G mode and $2D$ mode, respectively [32]. Furthermore, the G peak could be divided into two components, the lower frequency peak (G^-) located at 1571 cm^{-1} (m-SWCNTs) and 1569 cm^{-1} (s-SWCNTs) associated with vibrations along the circumferential direction, whereas the higher frequency peak (G^+) located at 1589 cm^{-1} (m-SWCNTs) and 1592 cm^{-1} (s-SWCNTs) attributed to vibrations along the directions of the tube axis [33]. In addition, the visible high G/D ratio for both m- and s-SWCNTs networks also proved a high purity and a low concentration of innate defects.

A typical aryl diazonium salt of 4-BBDT was employed to chemical functionalization of the m- and s-SWCNTs networks, respectively. As illustrated in the schematic diagram in Fig. 2a, after addition 4-BBDT into the SWCNTs suspension under the alkaline environment, the diazonium salts trend to extract electrons from the sidewall of nanotubes accompanied by releasing N_2 gas and finally generate the covalent aryl bonds. However, only the electrons

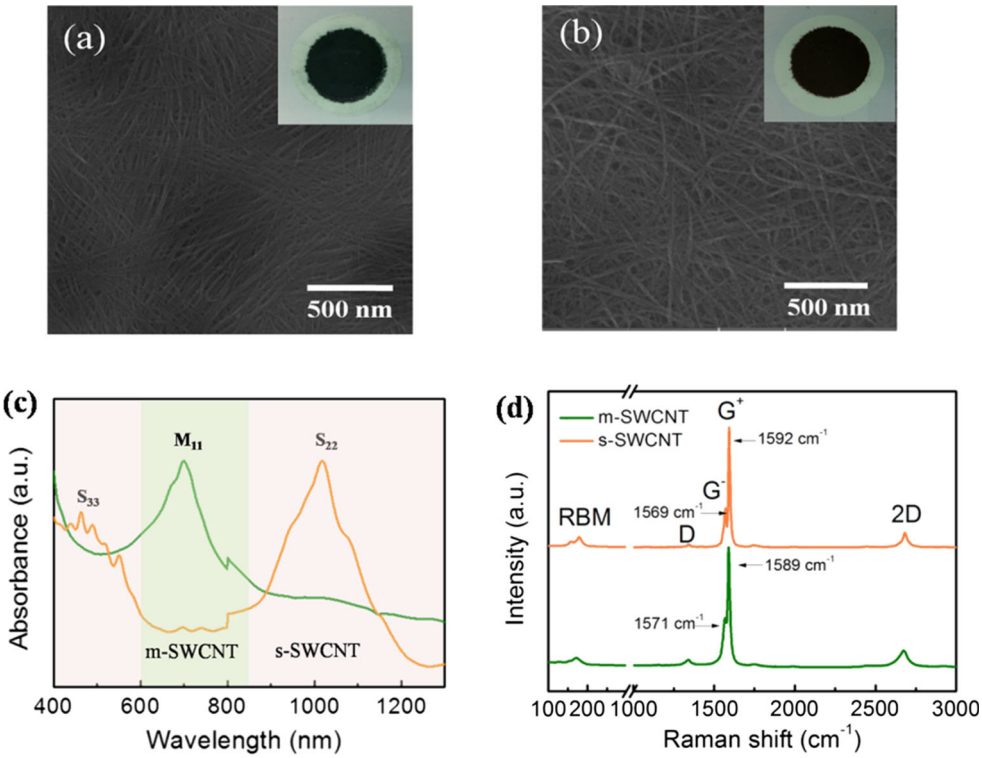

Figure 1 The representative SEM image of high-purity SWCNTs networks **a** m-SWCNTs and **b** s-SWCNTs, insets showing their digital photographs, respectively; **c** the corresponding absorption spectrum of m- and s-SWCNTs dispersions; **d** the Raman spectrum of m- and s-SWCNTs networks under the laser wavelength of 514 nm.

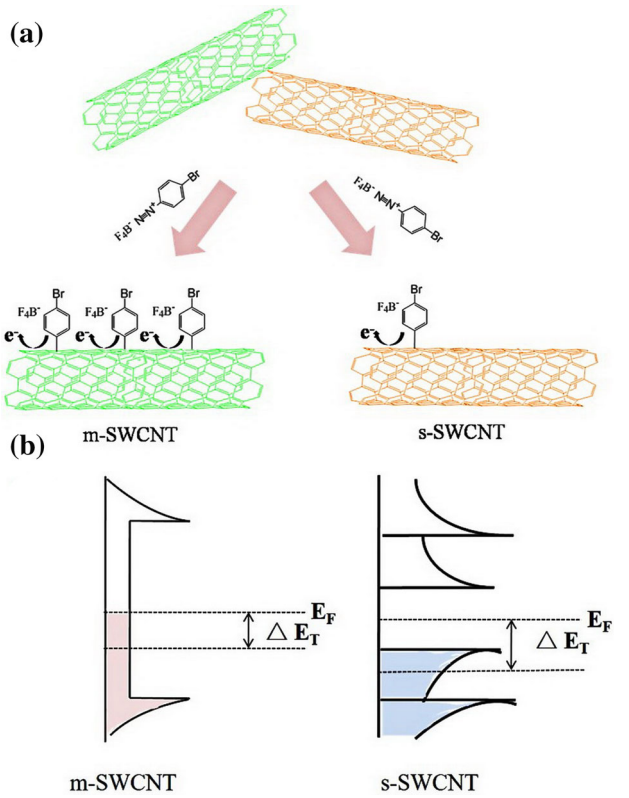

Figure 2 **a** Schematic diagram of the reaction process between SWCNTs and 4-BBDT; **b** schematic diagram of the *DOS* of m-SWCNTs and s-SWCNTs.

possess high affinity (low energy difference based on Fermi level, ΔE_T) locating near the Fermi level are available for the chemical reaction [29]. According to the DOS of m- and s-SWCNTs (seen in Fig. 2b), the electrons of m-SWCNTs located near the Fermi level are more than those of s-SWCNTs, indicating the reaction probability is significantly higher for m-SWCNTs compared with s-SWCNTs. Hence, 4-BBDT showed chemical selectivity against electronic type of SWCNTs.

The Raman spectrum of the corresponding chemically functionalized SWCNTs networks with different amounts of 4-BBDT is illustrated in Fig. 3. Since the *D* band involves the resonant phonon scattering of an electron by a defect that breaks the basic symmetry of the graphene plane [29], the intensity change of the *D* mode is an effective indicator to monitor the process of covalent functionalization. Generally, the value of *G*/*D* ratio is more frequently used instead of the absolute intensity value of *D* mode. After grafting of 4-BBDT on the sidewall of m- and s-SWCNTs, the shape of the *G* mode, which reflected the vibrations of carbon atoms in plane, was not changed obviously. This was demonstrated the basic framework of nanotubes was not destroyed after chemical functionalization with 4-BBDT. On the contrary, the intensity of *D* band was

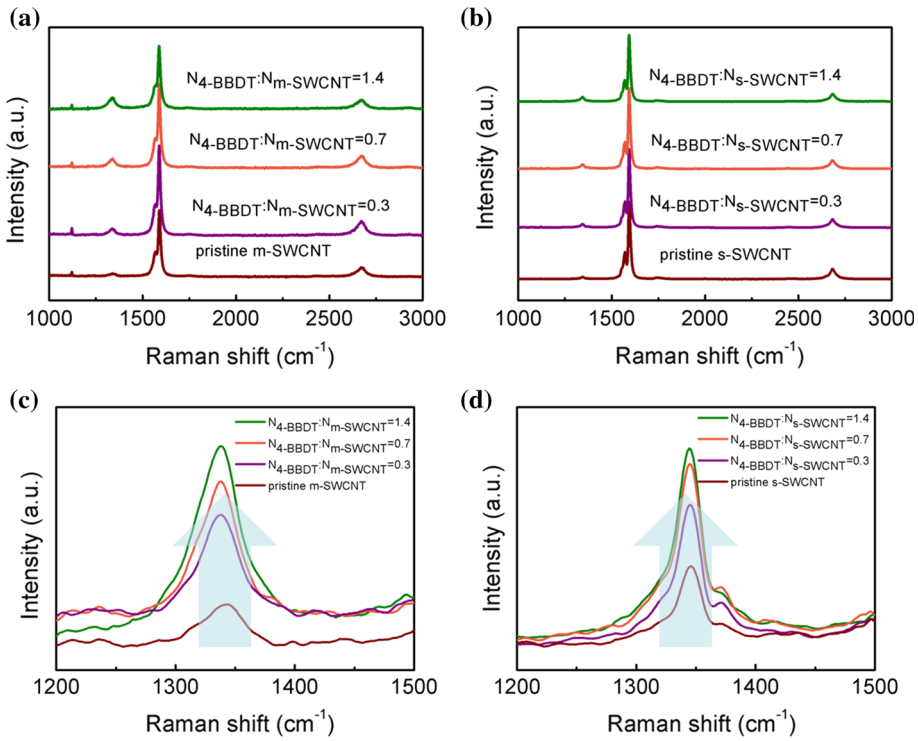

Figure 3 Raman spectrum of the pristine SWCNTs and the chemically treated SWCNTs networks as a function of the amount of 4-BBDT **a**, **c** m-SWCNTs; **b**, **d** s-SWCNTs.

prominently increased, leading to decrease in G/D ratio. Furthermore, the deteriorate degree of the G/D ratio was severer with increment of 4-BBDT, indicating the functionalization degree was increased. In specific, the G/D ratio of pristine m-SWCNTs networks was 17.5, and it was decreased to 4.7 with the molar ratio of 4-BBDT/m-SWCNTs fixed at 1.4 (73% descent), demonstrating a heavy level of functionalization degree. As a comparison, the G/D ratio of s-SWCNTs networks was decreased from 36.8 to 14.4 after the same amount of 4-BBDT treatment (60% descent), revealing that the m-SWCNTs is prior to react with 4-BBDT than s-SWCNTs. In further, on the basis of the literature that chemical functionalized with aryl diazonium salts [34], we estimated the degree of functionalization numerically from the relationship between the stoichiometry ratios (the number of carbon atoms per one functional group) and change rate of G/D $\left(\Delta\left(\frac{G}{D}/\frac{G}{D}\right)\right)$. As a consequence, in the case of m-SWCNTs, the molar ratios of $N_{4\text{-BBDT}}/N_{\text{m-SWCNT}} = 0.3, 0.7, 1.4$ corresponding to the number of carbon atoms per one functional group are 60, 45 and 27, respectively. As for s-SWCNTs, the stoichiometry ratios are 74, 56 and 47, respectively, under the same molar ratios.

The absorption spectrum of chemically functionalized m- and s-SWCNTs networks with a series of content of 4-BBDT is displayed in Fig. 4. After addition of 4-BBDT into m- and s-SWCNTs suspensions, both the characteristic peaks of m-SWCNTs (the first exciton absorption transition, M_{11}) and s-SWCNTs (the second exciton absorption transition, S_{22}) were initiated to bleach and became broader. Since the characteristic peaks interrelated with the valence electrons of each distinct nanotube, the grafting of 4-BBDT on the sidewall of SWCNTs leading to the localization of free electrons further decreased the absorption characteristic peaks. Similar to Raman spectrum, the decline degree of the absorption characteristic peaks was increased as a function of 4-BBDT, indicating an increment of functionalization degree.

The TE properties of pristine m- and s-SWCNTs networks were investigated as a pioneer. For Seebeck coefficient measurement, the thin films were cut into 20 × 20 mm strips, and the representative AFM micrograph of s-SWCNTs network are displayed in the inset of Fig. 5, revealing a high quality of SWCNTs networks without impurities. After the creation temperature gradient artificially, the measured potential differences were plotted as a function ΔT, and the Seebeck coefficient was acquired from the slope of this curve. As can be seen from Fig. 5, it clearly exhibited a substantial difference between

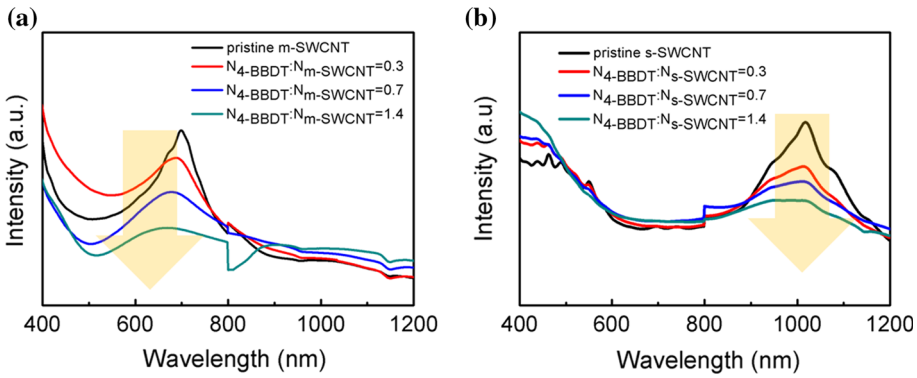

Figure 4 Absorption spectrum of the pristine SWCNTs and the chemically treated SWCNTs networks as a function of the amount of 4-BBDT **a** m-SWCNTs; **b** s-SWCNTs.

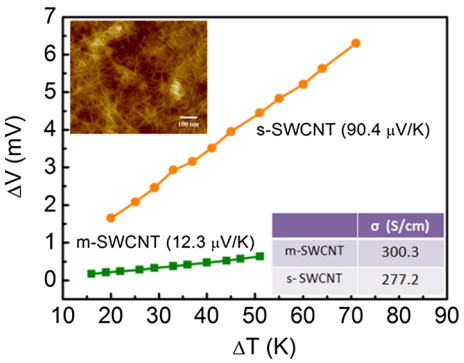

Figure 5 The measured V_{TEP} as a function of ΔT for m- and s-SWCNTs networks, inset displaying the measured electrical conductivity of m- and s-SWCNTs networks (bottom right), and representative AFM micrograph of s-SWCNTs network (top left).

these two monodispersed SWCNTs networks, that is, the Seebeck coefficient of s-SWCNTs was almost 7 times higher than that of m-SWCNTs. Actually, the Seebeck coefficient can be approximately expressed as Eq. (1) in the low-temperature range:

$$S(E_f) = -\frac{\pi^2}{3}\frac{\kappa_B^2 T}{e}\left[\frac{\partial \ln[N(E)]}{\partial E} + \frac{\partial \ln[D(E)]}{\partial E}\right]_{E=E_f} \quad (1)$$

where E is the energy, E_f is the Fermi level energy, k_B is the Boltzmann constant, and T is the absolute temperature. The first term in the bracket is the ballistic contribution to the Seebeck coefficient derived from the shape of DOS ($N(E)$), and the second term is the diffusive contribution derived from the energy dependence of the diffusion coefficient ($D(E)$) [35]. It is worth to mention that through the first-principles density functional theory (DFT) [25], the calculated intrinsic Seebeck coefficient of s-SWCNTs ($\sim$ 1285 μV K^{-1}, (7, 5)) was nearly one order of magnitude higher than that of m-SWCNTs ($\sim$ 125 μV K^{-1}, (9, 9)). Though the multiple of difference was consistent with our experiment results, there was a big deviation from the absolute values that cannot be ignored. The dramatically decreased absolute values of Seebeck coefficient stem from the heavily doped by the oxygen and water molecule in the air atmosphere, resulting in a p-type doping effect, which shifted the Fermi level toward the valence bands. Not only the observably influence on the Seebeck coefficient, the electrical conductivity was also severely affected. As a result, there was merely small difference of the electrical conductivity between heavily p-doped m- and s-SWCNTs networks, as seen in the inset of Fig. 5.

The TE properties as a function of the amount of 4-BBDT were investigated, as shown in Fig. 6. In both cases, the electrical conductivity of m- and s-SWCNTs networks became deterioration with increment of the diazonium salts, as shown in Fig. 6a. Generally, the electrical conductivity can be defined as

$$\sigma = ne\mu \quad (2)$$

where n is the carrier concentration, e is electron charge, and μ is carrier mobility [36]. As mentioned above, after mixing the monodispersed SWCNTs suspensions with 4-BBDT in alkaline environment, the diazonium salts spontaneously reacted with nanotubes and grafted onto the sidewall in terms of covalent aryl bonds. This process induced the hybrid orbital of C atoms changing from sp^2 to sp^3 [37]; hence, the free electrons were localized at the sidewall of nanotubes, resulting in a decrease in the concentration of free carriers. Furthermore, the grafting of molecular on the sidewall could be considered as impurity species, leading to increment of the phonon scattering and decline of the carrier mobility [38]. These two integrated factors caused the deterioration of the electrical conductivity of SWCNTs networks. However, due to the selectivity

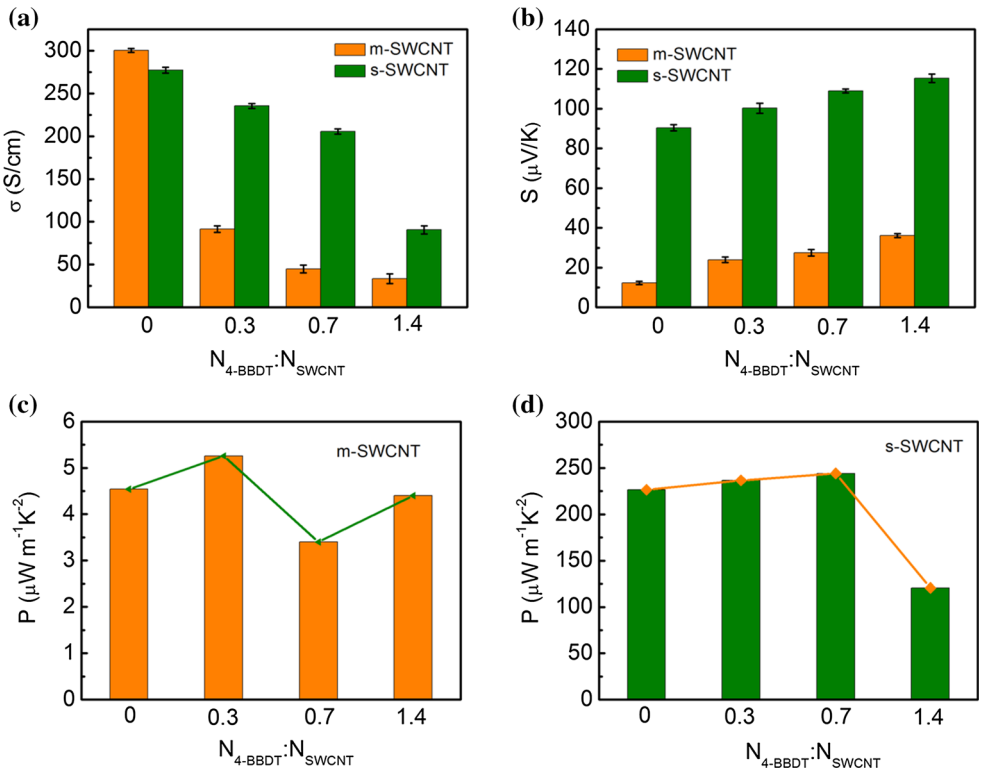

Figure 6 TE properties including **a** electrical conductivity and **b** Seebeck coefficient of the pristine SWCNTs and the chemically functionalized SWCNTs networks as a function of the content of 4-BBDT; power factor of chemically functionalized on **c** m-SWCNTs networks and **d** s-SWCNTs networks as a function of the content of 4-BBDT.

of the diazonium salts against electronic types of nanotubes, the reaction rate was much higher with m-SWCNTs than that of s-SWCNTs. As a consequence, the influence of the electrical conductivity was more evident on m-SWCNTs networks. In the case of the molar ratio of 4-BBDT/m-SWCNTs at 0.7, the electrical conductivity was decreased to 45 S cm^{-1} for m-SWCNTs networks, which was 85% damaged compared with the pristine sample, whereas the electrical conductivity was measured to be 205.7 S cm^{-1} for s-SWCNTs networks, which was only 26% damaged.

Different from the electrical conductivity, the chemical functionalization emerged a positive effect on the Seebeck coefficient for both types of SWCNTs networks. As displayed in Fig. 6b, the Seebeck coefficient was maintained to increase as a function of the amount of 4-BBDT. The covalent linkage of the aryl bonds on the nanotubes could be considered as phonon scattering centers. These obstacles can effectively filter out the low-energy carriers and allow the high-energy carriers to pass through, leading to the enhancement of the Seebeck coefficient [39]. Contrast to s-SWCNTs networks, the energy filtering effect was more remarkable on the m-SWCNTs networks owing to higher degree of functionalization. Therefore, the enhancement of Seebeck coefficient was greater for m-SWCNTs networks under the same condition. Under the molar ratio of 4-BBDT/s-SWCNTs fixed at 0.7, the value of Seebeck coefficient was 109 μV K^{-1} for s-SWCNTs networks, resulting in an improvement by 31% compared with the pristine sample, whereas the values of Seebeck coefficient for m-SWCNTs networks were enhanced from 12.3 to 27.5 μV K^{-1}, which was improved by 124% compared with the pristine sample.

The calculated power factors from electrical conductivity and Seebeck coefficient are shown in Fig. 6c, d. The power factor of pure m-SWCNTs networks was merely 4.54 μW m^{-1} K^{-2}; inspiringly, the value of pure s-SWCNTs networks reached up to 226.5 μW m^{-1} K^{-2}, which was higher than most of the organic TE materials. As we already know, the power factor is correlative with electrical conductivity and Seebeck coefficient, which are trade-off with each other. As a result, the power factor exhibited a fluctuation variation accompanied by the change in the functionalization degree. The maximum power factor obtained here was 244.2 μW m^{-1} K^{-2} with the molar ratio of 4-BBDT/s-SWCNTs to be 0.7, even higher than that of the pristine species. In addition, we also performed the same procedure on the

unsorted SWCNTs containing m-SWCNTs and s-SWCNTs randomly with purity higher than 95% (purchased from Chengdu Organic Chemicals Co. Ltd.). The TE properties including electrical conductivity and Seebeck coefficient were displayed in Fig. S1 and Fig. S2. Expectably, the variation tendency is similar with that of monodispersed SWCNTs accompanied by the different functionalization degree. According to Fig. S3, the optimum power factor appeared at the molar ratio of 4-BBDT/SWCNTs to be 0.7. The maximum power factor of the unsorted SWCNTs is higher than that of m-SWCNTs, but much lower than that of s-SWCNTs species. Following these results, the s-SWCNTs networks and a variety of relevant chemically functionalized composites can be considered as ideal TE materials.

Conclusions

In summary, pure m-SWCNTs and s-SWCNTs networks were fabricated through facile vacuum filtration technique. With no observable difference of the electrical conductivity due to the heavily p-type doped by oxygen and water molecular, the Seebeck coefficient of s-SWCNTs networks was measured to be 90.4 $\mu V\ K^{-1}$, which was 7.3 times higher than that of m-SWCNTs (12.3 $\mu V\ K^{-1}$). A typical diazonium salt of 4-BBDT was selected to chemical functionalization of the monodispersed SWCNTs. Due to the reaction selectivity against electronic types of nanotubes, the deterioration of the electrical conductivity for m-SWCNTs networks was much fiercer than that of s-SWCNTs species. On the contrary, it demonstrated a positive impact on the Seebeck coefficient after grafting the functional groups on the sidewall of nanotubes owing to the energy filtering effect. Experimentally, the maximum power factor was as high as 244.2 $\mu W\ m^{-1}\ K^{-2}$ under the optimum condition, which is higher than most of the organic TE materials. Accordingly, we consider that the pure s-SWCNTs and a variety of relevant chemically functionalized composites were ideal candidate for future TE applications.

Acknowledgements

This work was supported by National Natural Science Foundation of China (No: 51602306) and Venture & Innovation Support Program for Chongqing Overseas Returnees.

Compliance with ethical standards

Conflict of interest The authors declare that they have no conflict of interest.

Electronic supplementary material: The online version of this article (https://doi.org/10.1007/s10853-018-2063-4) contains supplementary material, which is available to authorized users.

References

[1] Nicola FD, Salvato M, Cirillo C et al (2016) 100% internal quantum efficiency in polychiral single-walled carbon nanotube bulk heterojunction/silicon solar cells. Carbon 114:402–410

[2] Liu YP, Jung E, Wang Y et al (2014) "Quasi-freestanding" graphene-on-single walled carbon nanotube electrode for applications in organic light-emitting diode. Small 10:944–949

[3] Chen Z, Zhu F, Wei Y et al (2008) Scanning focused laser activation of carbon nanotube cathodes for field emission flat panel displays. Nanotechnology 19:135703/1–135703/4

[4] Li HP, Tang YF, Guo WM et al (2016) Polyfluorinated electrolyte for fully printed carbon nanotube electronics. Adv Funct Mater 26:6914–6920

[5] Bucella SG, Salazar-Rios JM, Derenskyi V et al (2016) Inkjet printed single-walled carbon nanotube based ambipolarand unipolar transistors for high-performance complementary logic circuits. Adv Electron Mater 2:1600094/1–1600094/6

[6] Kumar D, Jha P, Chouksey A et al (2016) 4-(Hexafluoro-2-hydroxy isopropyl)aniline functionalized highly sensitive flexible SWCNT sensor for detection of nerve agent simulant dimethyl methylphosphonate. Mater Chem Phys 181:487–494

[7] Piao M, Joo MK, Choi JH et al (2015) Evaluation of power generated by thermoelectric modules comprising a p-type and n-type single walled carbon nanotube composite paper. RCS Adv 5:78099–78103

[8] Piao M, Na J, Choi J et al (2013) Increasing the thermoelectric power generated by composite films using chemically functionalized single-walled carbon nanotubes. Carbon 62:430–437

[9] Skakalova V, Kaiser AB, Woo YS et al (2006) Electronic transport in carbon nanotubes: from individual nanotubes to thin and thick networks. Phys Rev B 74:085403/1–085403/10

[10] Puchades I, Lawlor CC, Schauerman CM et al (2015) Mechanism of chemical doping in electronic-type-separated single wall carbon nanotubes towards high electrical conductivity. J Mater Chem C 3:10256–10266

[11] Dettlaff-Weglikowska U, Skakalova V, Jhang SH et al (2005) Effect of $SOCl_2$ treatment on electrical and mechanical properties of single-wall carbon nanotube networks. J Am Chem Soc 127:5125–5131

[12] Simoneau LP, Villeneuve J, Aguirre CM et al (2013) Influence of statistical distributions on the electrical properties of disordered and aligned carbon nanotube networks. J Appl Phys 114:114312/1–114312/8

[13] Avouris P (2002) Carbon nanotube electronics. Chem Phys 281:429–445

[14] Snyder GJ, Toberer ES (2008) Complex thermoelectric materials. Nat Mater 7:105–114

[15] Shimizu S, Iizuka T, Kanahashi K et al (2016) Thermoelectric detection of multi-subband density of states in semiconducting and metallic single-walled carbon nanotubes. Small 12:3388–3392

[16] Zhang L, Sun DM, Hou PX et al (2017) Selective growth of metal-free metallic and semiconducting single-wall carbon nanotubes. Adv Mater 29:1605719/1–1605719/9

[17] Phillips AB, Heben MJ (2015) Activated complex model and surfactant reorganization during SWCNT separations on hydrogels. Carbon 95:330–337

[18] Yanagi K, Udoguchi H, Sagitani S et al (2010) Transport mechanisms in metallic and semiconducting single-wall carbon nanotbue networks. ACS Nano 4:4027–4032

[19] Jackson RK, Munro A, Nebesny K et al (2010) Evaluation of transparent carbon nanotube networks of homogeneous electronic type. ACS Nano 4:1377–1384

[20] Moriarty GP, Wheeler JN, Yu C et al (2012) Increasing the thermoelectric power factor of polymer composites using a semiconducting stabilizer for carbon nanotubes. Carbon 50:885–895

[21] Zhao WY, Fan SF, Xiao N et al (2012) Flexible carbon nanotube papers with improved thermoelectric properties. Energy Environ Sci 5:5364–5369

[22] Piao M, Kim G, Kennedy GP et al (2013) Thermoelectric properties of single walled carbon nanotube networks in polycarbonate matrix. Phys Status Solidi B 250:1468–1473

[23] Wu GB, Gao CY, Chen GM et al (2016) High-performance organic thermoelectric modules based on flexible films of a novel n-type single-walled carbon nanotube. J Mater Chem A 4:14187–14193

[24] Piao M, Alam MR, Kim G et al (2012) Effect of chemical treatment on the thermoelectric properties of single walled carbon nanotube networks. Phys Status Solidi B 249:2353–2356

[25] Avery AD, Zhou BH, Lee J et al (2016) Tailored semiconducting carbon nanotube networks with enhanced thermoelectric properties. Nat Energy 1:16033/1–16033/9

[26] Piao M, Joo MK, Na J et al (2014) Effect of intertube junctions on the thermoelectric power of monodispersed single walled carbon nanotube networks. J Phys Chem C 118:26454–26461

[27] Rahmanifar E, Yoosefian M, Karimi-Maleh H (2016) Electronic properties and reactivity trend for defect functionalization of single-walled carbon nanotube with B, Al, Ga atoms. Synth Met 221:242–246

[28] Kim DH, Jin JE, Piao M et al (2014) Electrical percolation characteristics of metallic single-walled carbon nanotube networks by vacancy evolution. Phys Chem Chem Phys 16:18370–18374

[29] Strano MS, Dyke CA, Usrey ML et al (2003) Electronic structure control of single-walled carbon nanotube functionalization. Science 301:1519–1522

[30] Gontijo RN, Safar GAM, Righi A et al (2017) Quantifying (n, m) species in single-wall carbon nanotubes dispersions by combining Raman and optical absorption spectroscopies. Carbon 115:681–687

[31] Li N, Ma YF, Wang B et al (2011) Synthesis of semiconducting SWCNTs by arc discharge and their enhancement of water splitting performance with TiO_2 photocatalyst. Carbon 49:5132–5141

[32] Grimm S, Schießl SP, Zakharko Y et al (2017) Doping-dependent G-mode shifts of small diameter semiconducting single-walled carbon nanotubes. Carbon 118:261–267

[33] Dresselhaus MS, Dresselhaus G, Jorio A et al (2002) Raman spectroscopy on isolated single wall carbon nanotubes. Carbon 40:2043–2061

[34] Bahr JL, Yang J, Kosynkin DV et al (2001) Functionalization of carbon nanotubes by electrochemical reduction of aryl diazonium salts: a bucky paper electrode. J Am Chem Soc 123:6536–6542

[35] Zuev YM, Chang W, Kim P (2009) Thermoelectric and magnetothermoelectric transport measurement of graphene. Phys Rev B 102:096807/1–096807/4

[36] Xiong JH, Jiang FX, Shi H et al (2015) Liquid exfoliated graphene as dopant for improving the thermoelectric power factor of conductive PEDOT:PSS nanofilm with hydrazine treatment. ACS Appl Mater Interfaces 7:14917–14925

[37] Bahr JL, Tour JM (2002) Covalent chemistry of single-wall carbon nanotubes. J Mater Chem 12:1952–1958

[38] Minnich AJ, Dresselhaus MS, Ren ZF et al (2009) Bulk nanostructured thermoelectric materials: current research and future prospects. Energy Environ Sci 2:466–479

[39] Choi J, Lee JY, Lee SS et al (2016) High-performance thermoelectric paper based on double carrier-filtering processes at nanowire heterojunctions. Adv Energy Mater 6:1502181/1–1502181/8